

# Quantum Transport in a Nanosize Silicon-on-Insulator Metal-Oxide-Semiconductor Field Effect Transistor

M. D. Croitoru<sup>†</sup>, V. N. Gladilin<sup>†</sup>, V. M. Fomin<sup>†</sup>, J. T. Devreese<sup>‡</sup>

*Theoretische Fysica van de Vaste Stoffen (TFVS),*

*Universiteit Antwerpen (UIA), Universiteitsplein 1, B-2610 Antwerpen, Belgium*

W. Magnus, W. Schoenmaker, and B. Sorée

*IMEC, B-3001 Leuven, Belgium*

(Dated: March 7, 2019)

An approach is developed for the determination of the current flowing through a nanosize silicon-on-insulator (SOI) metal-oxide-semiconductor field-effect transistors (MOSFET). The quantum mechanical features of the electron transport are extracted from the numerical solution of the quantum Liouville equation in the Wigner function representation. Accounting for electron scattering due to ionized impurities, acoustic phonons and surface roughness at the Si/SiO<sub>2</sub> interface, device characteristics are obtained as a function of a channel length. From the Wigner function distributions, the coexistence of the diffusive and the ballistic transport naturally emerges. It is shown that the scattering mechanisms tend to reduce the ballistic component of the transport. The ballistic component increases with decreasing the channel length.

## I. INTRODUCTION

Down scaling MOSFETs to their limiting sizes is a key challenge of the semiconductor industry. Detailed simulations that capture the transport and the quantum mechanical effects that occur in these devices can complement experimental work in addressing this challenge. Furthermore, a conceptual view of the nanoscale transistor is needed to support the interpretation of the simulations and experimental data as well as to guide further experimental work. The objective of this work is to provide such a view by formulating a detailed quantum-mechanical transport model and performing extensive numerical simulations. We develop a model along these lines for the nanosize SOI, or thin film MOSFET, since the suppression of the short-channel effect seems to be most adequately addressed by this technology. Therefore, understanding the SOI MOSFET including its quantum-mechanical transport properties is urgently needed. In this work, we restrict our attention to the steady-state current-voltage characteristics.

The SOI MOSFET<sup>1</sup> is a transistor, built on a thin silicon layer, which is separated from the substrate by an insulating layer (Fig. 1). In the nanoscale transistor, we have to optimize device functionality and reliability. To achieve this goal, we need to suppress any short-channel effects as much as possible. These effects include threshold voltage variations versus channel length and the drain-induced barrier lowering effect, i.e. a drain voltage dependence of threshold voltage, which complicates transistor design at a circuit level. Frank *et al.*<sup>2</sup> recently showed, that increasing the channel doping concentration,  $N_{CH}$ , suppresses short-channel effects. The integration of the down-scaled devices requires that the gate insulating layer thickness should be reduced and/or higher dielectric constant of the insulator are implemented.

Si-based MOSFETs with typical sizes about 100 nm have found an application in highly integrated systems. Mechanisms of the electron transport in these devices differ from those in the devices of 50 nm and below. The 'conventional' devices are described by the Boltzmann transport equation and approximation thereof. This theories focus on scattering-dominant transport, which typically occurs in long channel devices. On the contrary, in a structure with a characteristic size of the order of the mean free path, the electron transport is essentially quasi-ballistic.

To describe the electron transport through a nanoscale transistor, a quantum-mechanical treatment is required. This includes the following approaches: the non-equilibrium Green's function formalism of Keldysh and Kadanoff-Baym<sup>3,4,5,6,7,8,9,10,11,12</sup>, the Pauli master equation method<sup>13,14,15</sup>, the full density matrix method<sup>16,17</sup> and Wigner function method<sup>18,19,20,21,22,23,24</sup>.

The main goal of the present work is the investigation of quantum transport in a nanosize MOSFET. Consequently, quantum effects such as quantum reflection and quantum tunnelling, occur in the electron transport. Simultaneously, electron scattering should be taken into account. Due to a low electron-scattering rate, the sub-50 nm devices are expected to offer higher speed performance than the conventional devices do. In a conventional MOSFET, the conductance is determined by the scattering rate of electrons in the channel, and the velocity of charge carriers is limited to a maximal value of about  $10^7$  cm/s. In MOSFETs with the channel length less than the mean free path, a velocity overshoot effect occurs<sup>25</sup>. The small length of the channel results into an increased on-state current and a reduced gate capacitance. For example, in Ref.<sup>26</sup> the fabrication of sub-0.1  $\mu$ m MOSFETs was reported. The resulting devices demonstrate a rather good performance in a wide range of temperatures.

In<sup>24</sup>, a flexible two-dimensional model has been developed, that optimally combines analytical and numerical methods and describes the key features of cylindrical SOI MOSFET devices. The theoretical tools to describe the quantum transport features involve the Wigner distribution function formalism<sup>22</sup>, in which a Boltzmann collision term representing acoustics phonons, impurity and surface-roughness scattering was incorporated. Therefore this model is capable to probe the competition between three effects: quantum reflection, quantum tunnelling and phase de-coherence due to elastic scattering. The Wigner function formalism offers many advantages for quantum modelling<sup>27,28</sup>. First, it is a phase-space distribution, similar to classical distributions. Because of the phase-space nature of the distribution, it is conceptually possible to use the correspondence principle in order to determine, where quantum corrections enter the problem. At the boundaries, the phase-space description allows for separation of incoming and outgoing components of the distribution, which therefore permits the modelling an ideal contact, and hence an open system<sup>20</sup>. By coupling the equation for the Wigner function to the Poisson equation, we obtain a fully-self-consistent model of the SOI MOSFET.

This paper is organized as follows : in Section II, a description of the system is presented in terms of a one-electron Hamiltonian. In Section III the quantum Liouville equation satisfied by the electron density matrix is transformed into a set of one-dimensional equations for partial Wigner functions. The boundary conditions for the Wigner function are considered in Section IV. The ballistic regime of the structure described in Section V. A one-dimensional collision term is derived in Section VI, in which we extend earlier work<sup>24</sup> by also including scattering due to interface roughness. In Section VII, we describe a numerical model to solve the equations for the Wigner function. In Section VIII, the results of the numerical calculations are discussed.

## II. THE HAMILTONIAN OF THE SYSTEM

We consider a  $n$ -channel SOI MOSFET structure. When a positive gate voltage is applied, electrons in the channel are confined to a narrow inversion layer near Si/SiO<sub>2</sub> interface. The current flows in the  $z$ -direction, the confinement is in the  $x$ -direction, and the width of the transistor is found along the  $y$ -direction. The source and drain regions with the lengths  $L_S$  and  $L_D$ , respectively, are  $n$ -doped by phosphorus with concentration  $N_D$ , whereas the  $p$ -doped channel with the length  $L_{CH}$  has concentration  $N_A$  of boron acceptors. The lateral surface of the semiconductor brick in the channel region is covered by the SiO<sub>2</sub> oxide layer, while the aluminum gate overlays the oxide layer.

In the semiconductor, the electron motion is determined by the following Hamiltonian :

$$\hat{H} = \sum_j \hat{H}_j$$

$$\hat{H}_j = -\frac{\hbar^2}{2m_j^{xx}} \frac{\partial^2}{\partial x^2} - \frac{\hbar^2}{2m_j^{yy}} \frac{\partial^2}{\partial y^2} - \frac{\hbar^2}{2m_j^{zz}} \frac{\partial^2}{\partial z^2} + V(\mathbf{r}) , \quad (1)$$

where  $\mathbf{r} = (x, y, z)$ ;  $V(\mathbf{r}) = V_B(\mathbf{r}) + V_e(\mathbf{r})$  is the potential energy associated with the energy barrier and the electrostatic field;  $m_j^{xx}$ ,  $m_j^{yy}$  and  $m_j^{zz}$  are the effective masses of the motion along the  $x$ ,  $y$  and  $z$ -axes, respectively, of an electron of the  $j$ -th valley.

The Schrödinger equation is solved within an effective mass approximation. It is assumed that Si/SiO<sub>2</sub> interface is parallel to the (100) plane. The conduction band in bulk silicon can be represented by six equivalent ellipsoids. When an electric field is applied in the [100]-direction, these six equivalent minima split into two sets of subbands<sup>29</sup>. The first set of subbands (unprimed) is two fold degenerate and represents those ellipsoids that respond with a heavy effective mass in the direction of the applied electric field. Because of the heavier mass, the ‘unprimed’ subbands have relatively lower bound-state energies, as compared to the ‘primed’ subbands and are therefore primarily occupied by electrons<sup>30</sup>.

The electrostatic potential energy  $V_e(\mathbf{r})$  satisfies Poisson’s equation

$$\nabla \cdot [\varepsilon_i \nabla V_e(\mathbf{r})] = \frac{e^2}{\varepsilon_0} \left( -n(\mathbf{r}) + N_D(\mathbf{r}) - N_A(\mathbf{r}) \right) , \quad i = 1, 2 , \quad (2)$$

where  $\varepsilon_1$  and  $\varepsilon_2$  are the dielectric constants of the semiconductor and oxide layers, respectively;  $n(\mathbf{r})$ ,  $N_D(\mathbf{r})$  and  $N_A(\mathbf{r})$  are the concentrations of electrons, donors and acceptors, respectively. The barrier potential is non-zero in both oxide layers, and its value is denoted by a constant  $V_B$ . In our calculations, we assume that the source electrode is grounded whereas the potentials at the drain and gate electrodes equal  $V_D$  and  $V_G$  respectively. The system is assumed to be uniform in the  $y$ -direction. Consequently, the electron density is constant along the  $y$ -axis and the edge effects in that direction are supposed to be negligible.

The study of the charge distribution in the cylindrical MOSFET with closed gate electrode in the state of the thermodynamical equilibrium (see Ref.<sup>31</sup>) has shown that the concentration of holes is much lower than that of

electrons, so that electron transport is found to provide the main contribution to the current flowing through the SOI MOSFET. For that reason, holes are neglected in the present transport calculations.

### III. THE QUANTUM LIOUVILLE EQUATION

In order to study the device architecture starting from the Wigner function formalism, an equation is needed that describes the response of the Wigner function to changing external conditions. The time evolution of the Wigner function is derived from the quantum Liouville equation by applying the Wigner-Weyl transformation. Neglecting inter-valley transitions in the conduction band, the one-electron density matrix can be written as

$$\rho(\mathbf{r}, \mathbf{r}') = \sum_j \rho_j(\mathbf{r}, \mathbf{r}') , \quad (3)$$

where  $\rho_j(\mathbf{r}, \mathbf{r}')$  is the density matrix of electrons residing in the  $j$ -th valley satisfying the quantum Liouville equation

$$\hbar \frac{\partial \hat{\rho}_j}{\partial t} = [\hat{H}_j, \hat{\rho}_j] . \quad (4)$$

In order to impose the boundary conditions for the density matrix at the electrodes, it is convenient to describe the quantum transport along the  $z$ -axis in a phase-space representation. For that purpose, we expand the  $j$ -valley density matrix into a series with respect to a complete set of orthonormal functions  $\Psi_{jps}(x, y, z)$  and rewrite the density matrix  $\rho_j$  in terms of  $\zeta = (z + z')/2$  and  $\eta = z - z'$  coordinates as

$$\rho_j(\mathbf{r}, \mathbf{r}') = \sum_{psp's'} \frac{1}{2\pi} \int_{-\infty}^{+\infty} dk \exp(ik\eta) f_{jpsp's'}(\zeta, k) \Psi_{jps}(x, y, z) \Psi_{jp's'}^*(x', y', z') . \quad (5)$$

According to the symmetry of the system, these functions take the following form :

$$\Psi_{jps}(x, y, z) = \frac{1}{\sqrt{L_y}} \psi_{js}(x, z) \exp(ip_y) . \quad (6)$$

The functions  $\psi_{js}(x, z)$  are chosen to satisfy the equation

$$-\frac{\hbar^2}{2m_j^{xx}} \frac{\partial^2}{\partial x^2} \psi_{js}(x, z) + V(r, z) \psi_{js}(r, z) = E_{js}(z) \psi_{js}(x, z) \quad (7)$$

that describes the confined motion of an electron. Here  $E_{js}(z)$  are the eigenvalues of Eq. (7) for a given value of the  $z$ -coordinate that appears as a parameter. It will be shown, that  $E_{js}(z)$  plays the role of an effective potential in the channel, and that  $\Psi_{jps}(x, y, z)$  is the corresponding wavefunction of the motion along the  $x$ -axis at a fixed  $z$ . Substituting the expansion (5) into Eq. (4), and using Eq. (7), we arrive at the equation for  $f_{jpsp's'}(\zeta, k)$  :

$$\begin{aligned} \frac{\partial f_{jpsp's'}(\zeta, k)}{\partial t} = & -\frac{\hbar k}{m_j^{zz}} \frac{\partial}{\partial \zeta} f_{jpsp's'}(\zeta, k) + \frac{1}{\hbar} \int_{-\infty}^{+\infty} W_{jpsp's'}(\zeta, k - k') f_{jpsp's'}(\zeta, k') dk' \\ & - \sum_{s_1, s'_1} \int_{-\infty}^{+\infty} \hat{M}_{jpsp's'}^{s_1 s'_1}(\zeta, k, k') f_{jps_1 p' s'_1}(\zeta, k') dk' , \end{aligned} \quad (8)$$

where

$$W_{jpsp's'}(\zeta, k - k') = \frac{1}{2\pi i} \int_{-\infty}^{+\infty} d\eta (E_{jps}(\zeta + \eta/2) - E_{jp's'}(\zeta - \eta/2)) \exp(i(k' - k)\eta) , \quad (9)$$

$$\hat{M}_{jpsp's'}^{s_1 s'_1}(\zeta, k, k') = \frac{1}{2\pi} \int_{-\infty}^{+\infty} \left[ \delta_{s's'_1} \hat{\Gamma}_{ps_{s_1}}(\zeta + \eta/2, k') + \delta_{ss_1} \hat{\Gamma}_{ps's'_1}^*(\zeta - \eta/2, k') \right] \exp(i(k' - k)\eta) d\eta , \quad (10)$$

$$\hat{\Gamma}_{ps s_1}(\zeta + \eta/2, k') = \frac{\hbar}{2m_j^{zz}} b_{j s s_1}(\zeta + \eta/2) + \frac{\hbar}{2m_j^{zz}} c_{j s s_1}(\zeta + \eta/2) \left( -i \frac{\partial}{\partial \zeta} + 2k' \right), \quad (11)$$

$$\hat{\Gamma}_{ps' s'_1}^*(\zeta - \eta/2, k') = \frac{\hbar}{2m_j^{zz}} b_{j s s_1}(\zeta - \eta/2) + \frac{\hbar}{2m_j^{zz}} c_{j s s_1}(\zeta - \eta/2) \left( i \frac{\partial}{\partial \zeta} + 2k' \right)$$

and

$$b_{j s s_1}(z) = \int \psi_{j s}^*(x, z) \frac{\partial^2}{\partial z^2} \psi_{j s_1}(x, z) dx, \quad (12)$$

$$c_{j s s_1}(z) = \int \psi_{j s}^*(x, z) \frac{\partial}{\partial z} \psi_{j s_1}(x, z) dx, \quad (13)$$

$$E_{j p s}(z) = E_{j s}(z) + \frac{\hbar^2 p^2}{2m_j^{yy}}. \quad (14)$$

The first term in the right-hand side of Eq. (8) is derived from the kinetic-energy operator of the motion along the  $z$ -axis. It is exactly the same as the drift term of the Boltzmann equation. The second component plays the same role as the force term does in the Boltzmann equation. The last term in the right-hand side of Eq. (8) contains the kernel  $\hat{M}_{j p s p' s'}^{s_1 s'_1}(\zeta, k, k')$ , which mixes the functions  $f_{j p s p' s'}$  with different indices  $s, s'$ . This term appears because  $\psi_{j s}(x, z)$  are not eigenfunctions of the Hamiltonian (1).

#### IV. BOUNDARY CONDITIONS

To describe the behavior of the SOI MOSFET through solving Eq. (8), we need to specify the boundary conditions for the functions  $f_{j p s p' s'}(\zeta, k)$  that permit particles to enter and leave the system. The SOI MOSFET is described as an open system. Being part of an electrical circuit, it exchanges electrons with the circuit. For the present purposes, the term "open system" is used here to characterize a system that is connected to contacts (reservoirs of particles) and the interaction between the system and a contact necessarily involves a particle current through an interface between the system and contacts.

The quantum Liouville equation (in the Wigner-Weyl representation) is of the first order with respect to the coordinate  $\zeta$  and does not contain derivatives with respect to the momentum. The characteristics of the derivative term are lines of constant momentum, and we need to supply one and *only* one boundary value at some point on each characteristic, because the equation is of first order with respect to the coordinate  $\zeta$ . Thus, the Wigner function is a natural representation for an open system (SOI MOSFET). The implementation of the above described picture and the comparison of Eq. (5) with the corresponding expansion of the density matrix in the equilibrium state, leads to the following boundary conditions<sup>19,22,32</sup>:

$$\begin{aligned} f_{j m s m' s'}(0, k) &= 2\delta_{s s'} \delta_{m m'} [\exp \beta(E_{j s p k} - E_{\text{FS}}) + 1]^{-1}, & k > 0, \\ f_{j m s m' s'}(L, k) &= 2\delta_{s s'} \delta_{m m'} [\exp \beta(E_{j s p k} - E_{\text{FD}}) + 1]^{-1}, & k < 0, \end{aligned} \quad (15)$$

where the total energy is  $E_{j s p k} = \hbar^2 k^2 / 2m_j^{zz} + \hbar^2 p^2 / 2m_j^{yy} + E_{j s}(0)$  for an electron entering from the source electrode ( $k > 0$ ) and  $E_{j s p k} = \hbar^2 k^2 / 2m_j^{zz} + \hbar^2 p^2 / 2m_j^{yy} + E_{j s}(L)$  for an electron entering from the drain electrode ( $k < 0$ ). In Eq. (15)  $\beta = 1/k_B T$  is the inverse thermal energy, while  $E_{\text{FS}}$  and  $E_{\text{FD}}$  are the Fermi energy levels in the source and in the drain respectively. Note, that Eq. (15) meets the requirement of imposing only one boundary condition on the function  $f_{j p s p' s'}(\zeta, k)$  at a fixed value of  $k$  as Eq. (8) is a first-order differential equation with respect to  $\zeta$ .

#### V. BALLISTIC REGIME OF THE SOI MOSFET

The functions  $f_{j p s p' s'}(\zeta, k)$ , which are introduced in Eq. (5), are used in calculations of the current and the electron density. The expression for the electron density follows directly from the density matrix as  $n(\mathbf{r}) = \rho(\mathbf{r}, \mathbf{r})$ . In terms

of the functions  $f_{jpsp's'}(\zeta, k)$ , the electron density can be written as follows :

$$n(\mathbf{r}) = \frac{1}{2\pi} \sum_{jpsp's'} \int_{-\infty}^{+\infty} f_{jpsp's'}(z, k) dk \Psi_{jps}(x, y, z) \Psi_{jp's'}^*(x, y, z) . \quad (16)$$

The current density can be expressed in terms of the density matrix<sup>33</sup> :

$$\mathbf{J}(\mathbf{r}) = \sum_j \frac{e\hbar}{2m_j} \left( \frac{\partial}{\partial \mathbf{r}} - \frac{\partial}{\partial \mathbf{r}'} \right) \rho_j(\mathbf{r}, \mathbf{r}') \Big|_{\mathbf{r}=\mathbf{r}'} . \quad (17)$$

The total current passing through the cross-section of the structure at a point  $z$ , can be obtained by an integration over the transverse coordinates. Substituting the expansion (5) into Eq. (17) and integrating over  $x$  and  $y$ , we find

$$J = e \sum_{j,p,s} \frac{1}{2\pi} \int_{-\infty}^{+\infty} dk \frac{\hbar k}{m_j^{zz}} f_{jpsps}(z, k) - \frac{2e\hbar}{m_j^{zz}} \sum_{j,p,s < s'} c_{jss'}(z) \int_{-\infty}^{+\infty} dk \Im(f_{jpsps'}(z, k)) , \quad (18)$$

where  $\Im(f)$  is the imaginary part of  $f$ . The first term in the right-hand side of Eq. (18) is similar to the expression for a current of the classical theory<sup>33</sup>. The second term, which only depends on the non-diagonal functions  $f_{jpsps'}$ , takes into account the effects of intermixing between different states of the transverse motion.

Since  $\hat{M}_{jpsp's'}^{s_1 s'_1}$  couples functions  $f_{jpsp's'}(\zeta, k)$  with different quantum numbers ( $jps$ ), it can be interpreted as a collision operator, which describes transitions of electrons between different quantum states of the transverse motion. As shown in Ref.<sup>31</sup>, the third term in the right-hand side of Eq. (8) is significant only in the close vicinity of the  $p$ - $n$  junctions. Therefore, this term is assumed to give a small contribution to the charge and current densities. Using the above assumption, we can treat the last term in the right-hand side of Eq. (8) as a perturbation. Here after, we investigate the steady state of the system in a zeroth order approximation with respect to the operator  $\hat{M}_{jpsp's'}^{s_1 s'_1}$ . Neglecting the latter, one finds that, due to the boundary conditions (15), all non-diagonal functions  $f_{jpsp's'}(\zeta, k)$  ( $p \neq p'$  or  $s \neq s'$ ) are equal to zero<sup>24</sup>. Furthermore, summation over  $p$  in Eq. (8) gives

$$\frac{\hbar k}{m_j^{zz}} \frac{\partial}{\partial \zeta} f_{js}(\zeta, k) - \frac{1}{\hbar} \int_{-\infty}^{+\infty} W_{js}(\zeta, k - k') f_{js}(\zeta, k') dk' = 0 \quad (19)$$

with

$$f_{js}(\zeta, k) = \frac{1}{2\pi} \sum_p f_{jpsps}(\zeta, k) . \quad (20)$$

In Eq. (19) the following notation is used :

$$W_{js}(\zeta, k) = -\frac{1}{2\pi} \int_{-\infty}^{+\infty} (E_{js}(\zeta + \eta/2) - E_{js}(\zeta - \eta/2)) \sin(k\eta) d\eta . \quad (21)$$

The effective potential  $E_{js}(z)$  can be interpreted as the bottom of the subband ( $j, s$ ) in the channel. The function  $f_{js}(\zeta, k)$  is referred to as a partial Wigner function describing electrons, that are traveling through the channel in the inversion layer subband ( $j, s$ ).

## VI. ELECTRON SCATTERING

In this section, we consider the electron scattering due to acoustic phonons, impurities and surface roughness at the Si-SiO<sub>2</sub> interface. For this purpose, we introduce a Boltzmann-like single collision term<sup>33,34</sup>, which in the present case has the following form

$$\text{St } f_{jsmk} = \sum_{j's'p'k'} (P_{jspk,j's'p'k'} f_{j's'p'k'} - P_{jspk,j's'p'k'} f_{jspk}) . \quad (22)$$

As noted above, we have neglected all transitions between quantum states with different sets of quantum numbers  $j$  and  $s$ . In general, the density matrix has off-diagonal elements between different subbands in the presence of inter-subband scattering processes. But when the broadening of inverse layer levels due to inter-subband scattering is sufficiently small in comparison with subband energy separations, we can neglect such off-diagonal parts and use the transport equation (19), which becomes a set of decoupled equations for distribution functions associated with each subband  $(j, s)$ , i.e. in this case the electrons in the different subbands can be considered independent current carriers.

The transition rates depend upon the full set of quantum numbers of each three-dimensional state. Because the present calculations consider only the longitudinal momentum  $k$ , the scattering rates must be "projected" onto the one-dimensional model. To do so, we first assume that the distribution of electrons with respect to the motion along the  $y$ -direction is the normalized Maxwellian distribution at a fixed temperature, because in the source and drain contacts the distribution of electrons over the quantum states of the motion along the  $y$ -direction corresponds to an equilibrium distribution. Consequently, due to the symmetry of the system, it is reasonable to assume that across the whole structure the electron distribution is given by

$$f_{jspk}(\zeta) = f_{js}(\zeta, k) w_{jsp}, \quad (23)$$

where the integration measure

$$w_{jsp} = \sqrt{\frac{\hbar^2 \beta}{2m_j^{yy} \pi}} \exp\left(-\frac{\beta \hbar^2 p^2}{2m_j^{yy}}\right) dp \quad (24)$$

is the normalized Maxwellian distribution function with respect to the momentum  $p$ . The integration of Eq. (22) over the angular momentum gives the collision term

$$\text{St } f_{js}(\zeta, k) = \sum_{k'} (P_{js}(\zeta, k, k') f_{js}(\zeta, k') - P_{js}(\zeta, k', k) f_{js}(\zeta, k)) , \quad (25)$$

where

$$P_{js}(\zeta, k, k') = \sum_{pp'} P_{jspk, jsp'k'} w_{jsp'} \left(\frac{2\pi}{L_y}\right)^2 . \quad (26)$$

This collision term is directly incorporated into the quantum Liouville equation (19) as

$$\tilde{W}_{js}(\zeta, k, k') = W_{js}(\zeta, k - k') + \frac{L\hbar}{2\pi} \left( P_{js}(\zeta, k, k') - \delta_{k,k'} \sum_{k'} P_{js}(\zeta, k', k) \right) , \quad (27)$$

where  $\tilde{W}_{js}(z, k, k')$  is the modified force term in Eq. (19).

The scattering rates in the first Born approximation<sup>35</sup> are evaluated according to the Fermi's golden rule

$$P_{jsmk, jsm'k'} = \frac{2\pi}{\hbar} \left| \langle jsp'k' | \hat{H}_{\text{int}} | jspk \rangle \right|^2 \delta(E_{jsp'k'} - E_{jspk}) , \quad (28)$$

where  $\hat{H}_{\text{int}}$  is the Hamiltonian of the electron-phonon, the electron-impurity or electron-interface roughness interaction. The electron-electron interaction is taken into account by the Hartree potential in the single electron Hamiltonian.

Details of the scattering mechanisms are presented in Appendix.

## VII. NUMERICAL MODEL

The system under consideration consists of regions with high (the source and drain) and low (the channel) concentrations of electrons. The difference of the electron distribution in the corresponding regions would produce a considerable inaccuracy if we would have attempted to directly construct a finite-difference analog of Eq. (19). It is worth mentioning that, in the quasi-classical limit, i.e.  $E_{js}(\zeta + \eta/2) - E_{js}(\zeta - \eta/2) \approx \frac{\partial E_{js}(\zeta)}{\partial \zeta} \eta$ , Eq. (19) leads to the Boltzmann equation with an effective potential which has the following exact solution in equilibrium ( $E_F = E_{FS} = E_{FD}$ ):

$$f_{js}^{\text{eq}}(\zeta, k) = \frac{1}{\pi} \sum_m \left[ \exp \left( \beta \left( \frac{\hbar^2 k^2}{2m_j^{zz}} + E_{js}(\zeta) + \frac{\hbar^2 p^2}{2m_j^{yy}} - E_F \right) \right) + 1 \right]^{-1} . \quad (29)$$

For numerical calculations it is useful to write down the partial Wigner distribution function as  $f_{js}(\zeta, k) = f_{js}^{\text{eq}}(\zeta, k) + f_{js}^{\text{d}}(\zeta, k)$ . Inserting this into Eq. (19), one obtains the following equation for  $f_{js}^{\text{d}}(\zeta, k)$  :

$$\frac{\hbar k}{m_j^{\text{zz}}} \frac{\partial}{\partial \zeta} f_{js}^{\text{d}}(\zeta, k) - \frac{1}{\hbar} \int_{-\infty}^{+\infty} \tilde{W}_{js}(z, k, k') f_{js}^{\text{d}}(\zeta, k') dk' = B_{js}(\zeta, k), \quad (30)$$

where

$$B_{js}(\zeta, k) = \frac{1}{2\pi} \int_{-\infty}^{+\infty} dk' \int_{-\infty}^{+\infty} d\eta \left( E_{js}(\zeta + \frac{\eta}{2}) - E_{js}(\zeta - \frac{\eta}{2}) - \frac{\partial E_{js}(\zeta)}{\partial \zeta} \eta \right) \sin[(k - k')\eta] f_{js}^{\text{eq}}(\zeta, k'). \quad (31)$$

The unknown function  $f_{js}^{\text{d}}(\zeta, k)$  takes values of the same order throughout the whole system, and therefore is suitable for numerical computations. In the present work, we have used the finite-difference model, which is described in Ref.<sup>22,36</sup>. The position variable takes the set of discrete values  $\zeta_i = \Delta\zeta i$  for  $\{i = 0, \dots, N_\zeta\}$ . The values of  $k$  are also restricted to the discrete set  $k_p = (2p - N_k - 1)\Delta k/2$  for  $\{p = 1, \dots, N_k\}$ . The mesh spacing in the  $k$  space is

$$\Delta k = \frac{\pi\hbar}{N_k \Delta\zeta}. \quad (32)$$

The choice of discrete values for  $k$  follows from a desire to avoid the point  $k = 0$  and the need to satisfy a Fourier completeness relation. On a discrete mesh, the first derivative  $\frac{\partial f_{js}}{\partial \zeta}(\zeta_i, k_p)$  is approximated by the left-hand difference for  $k_p > 0$  and the right-hand difference for  $k_p < 0$ . It was shown in Ref.<sup>22</sup>, that such a choice of the finite-difference representation for the derivatives leads to a stable discrete model. Projecting the equation (30) onto the finite-difference basis gives a matrix equation  $\mathbf{L} \cdot \mathbf{f} = \mathbf{b}$ . In the matrix  $\mathbf{L}$ , only the diagonal blocks and one upper and one lower co-diagonal blocks are nonzero :

$$\mathbf{L} = \begin{pmatrix} A_1 & -U & 0 & \dots & 0 \\ -V & A_2 & -U & \dots & 0 \\ 0 & -V & A_3 & \dots & 0 \\ \vdots & \vdots & \vdots & \ddots & \vdots \\ 0 & 0 & 0 & \dots & A_{N_\zeta-1} \end{pmatrix}. \quad (33)$$

Here,  $A_i$ ,  $U$ , and  $V$  are  $N_k \times N_k$  matrices,

$$[A_i]_{pp'} = \delta_{pp'} \left( 1 + \frac{2m_j^{\text{zz}} \Delta\zeta}{\hbar^2 (2p - N_k - 1) \Delta k} \sum_{p''} \hbar P_{js}(k_{p''}, k_{p'}) \right) - \frac{2m_j^{\text{zz}} \Delta\zeta}{\hbar^2 (2p - N_k - 1) \Delta k} (W_{js}(\zeta_i, k_p - k_{p'}) + \hbar P_{js}(k_p, k_{p'})), \quad (34)$$

$$[U]_{pp'} = \delta_{pp'} \theta \left\{ \frac{N_k + 1}{2} - p \right\}, \quad [V]_{pp'} = \delta_{pp'} \theta \left\{ p - \frac{N_k + 1}{2} \right\}, \quad (35)$$

and the vectors are

$$[f_i]_p = f_{js}(\zeta_i, k_p), \quad \text{and} \quad [b_i]_p = B_{js}(\zeta_i, k_p), \quad i = 1, N_\zeta - 1, \quad p = 1, N_k. \quad (36)$$

A recursive algorithm is used to solve the matrix equation  $\mathbf{L} \cdot \mathbf{f} = \mathbf{b}$ . Invoking downward elimination, we are dealing with  $B_i = (A_i - V B_{i-1})^{-1} U$  and  $c_i = (A_i - V B_{i-1})^{-1} (b_i + V c_{i-1})$  ( $i = 1, \dots, N_\zeta$ ) as the relevant matrices and vectors. Then, upward elimination eventually yields the solution  $f_i = B_i f_{i+1} + c_i$  ( $i = N_\zeta - 1, \dots, 1$ ). If a particular index of a matrix or a vector is smaller than 1 or larger than  $N_\zeta - 1$ , the corresponding term is supposed to vanish.

In the channel, the difference between effective potentials  $E_{js}(\zeta)$  with different  $(j, s)$  is of the order of or larger than the thermal energy  $k_B T$ . Therefore, in the channel only the lowest few inversion layer subbands must be taken into account. In the source and drain, however, many quantum states  $(j, s)$  of the motion along the  $x$ -axis are strongly

populated by electrons. Therefore, we should account for all of them in order to calculate the charge distribution. Here, we can use the fact that, according to our approximation, the current flows only through the lowest subbands in the channel. Hence, only for these subbands the partial Wigner function of electrons is non-equilibrium. In other subbands, electrons are maintained in the state of equilibrium, even when a bias is applied. So, in Eq. (16) for the electron density, we can substitute functions  $f_{jpsps}(z, k)$  of higher subbands by corresponding equilibrium functions. Formally, adding and subtracting the equilibrium functions for the lowest subbands in Eq. (16), we arrive at the following equation for the electron density

$$n(\mathbf{r}) = n_{\text{eq}}(\mathbf{r}) + \frac{1}{L_y} \sum_{js} \int_{-\infty}^{+\infty} dk \left( f_{js}(z, k) |\psi_{js}(x; z)|^2 - f_{js}^{\text{eq}}(z, k) |\psi_{js}^{\text{eq}}(x; z)|^2 \right), \quad (37)$$

where  $n_{\text{eq}}(\mathbf{r})$  and  $\psi_{js}^{\text{eq}}(x; z)$  are the electron density and the wavefunction of the radial motion in the state of equilibrium respectively. The summation in the right-hand side of Eq. (37) is performed only over the lowest subbands. Since the electrostatic potential does not penetrate into the source and drain, we assume that the equilibrium electron density *in these regions* is described to sufficient accuracy by the Thomas-Fermi approximation :

$$n_{\text{eq}}(\mathbf{r}) = N_C \frac{2}{\sqrt{\pi}} F_{1/2}(\beta(eV(r, z) + E_F - E_C)), \quad (38)$$

where the Fermi integral is defined by

$$F_{1/2}(x) = \int_0^\infty \frac{\sqrt{t}}{\exp(t-x) + 1} dt. \quad (39)$$

Here  $N_C$  is the effective density of states in the conduction band and  $E_F$  denotes the Fermi level of the system in equilibrium.

## VIII. RESULTS AND DISCUSSION

For the numerical simulation of the SOI MOSFET we have fixed the geometrical parameters of the system as follows. The thicknesses of the semiconductor and oxide layers are chosen to be  $t_{\text{Si}} = 20$  nm and  $t_{\text{ox}} = 2$  nm respectively; the width of the MOSFET along the  $y$ -axis is taken to be 50 nm, the lengths of the drain and source are 20 nm each, while the barrier potential  $V_B$  at the Si/SiO<sub>2</sub> interface equals 3.2 eV. The values of the channel length considered for the numerical calculations are  $L_{\text{CH}} = 20, 30, 40$  nm. We further assume that the source electrode is grounded, whereas the potentials at the drain and gate electrodes equal  $V_D$  and  $V_G$  respectively. All numerical simulations are carried out with  $N_\zeta = 240$  and  $N_k = 120$ . The  $I - V$  characteristics are computed for a gate voltage  $V_G = 1.0$  V, while the drain voltage  $V_D$  varies from 0 to 1.0 V. The temperature of the system is  $T = 300$  K. The doping level of the source and drain regions is  $N_D = 10^{20}$  cm<sup>-3</sup>, whereas the channel is doped with an acceptor concentration  $N_A = 10^{18}$  cm<sup>-3</sup>. In calculations of the scattering the following values of parameters for Si are used:  $\Delta = 0.2, 0.4$  nm,  $\Lambda = 1.5$  nm<sup>29,37,38</sup>,  $\Xi_u = 9.2$  eV,  $\rho = 2.3283 \cdot 10^3$  kg/m<sup>3</sup>,  $v_0 = 8.43 \cdot 10^5$  cm/s<sup>39</sup>.

The simulation of the SOI MOSFET requires a self-consistent solution of three equations: (i) the Poisson equation (2); (ii) the Schrödinger equation yielding the wavefunctions describing the transverse motion in the  $x$ -direction (7); (iii) the equation obeyed by the partial Wigner distribution function (19). In the present calculations the eight lowest subbands are taken into account.

Fig. 2 illustrates the distribution of the electrostatic potential for  $V_D = 0.5$  V and for the value of the channel length  $L_{\text{CH}} = 30$  nm. Clearly, the main part of the applied gate voltage falls across the insulator while, due to the surface potential confinement, the current mainly flows in a thin layer near the Si/SiO<sub>2</sub> interface. At the  $p$ - $n$  junctions (source-channel and drain-channel) the electrons meet barriers across the whole semiconductor. These barriers persist even for high values of the applied voltage  $V_D$ .

In Fig. 3 the effective potential for the lowest inversion subband ( $j = 1, s = 1$ ) is plotted as a function of  $z$  for different values of the applied bias ranging from 0 to 0.5 V,  $V_G = 1$  V,  $L_{\text{CH}} = 30$  nm. In the case of ballistic transport (solid lines), the applied source-drain voltage sharply drops near the drain-channel junction. The scattering of electrons (dashed lines) smooths out the applied voltage, which is now varying almost linearly along the whole channel. The potential obtained by taking into account scattering is always higher than that of ballistic case. This can be explained by noticing that channel scattering locally increases the electron density and therefore enhances its capability of screening the applied gate voltage.



Fig. 4 shows the effective potential for the lowest inversion subband as a function of  $z$  for different values of the applied gate voltage  $V_G$  ranging from 0 to 1.0 V,  $V_D = 0.5$  V,  $L_{CH} = 30$  nm. The effective potential drop near the source-channel junction increases with increase gate voltage. This effect results into the potential barrier narrowing and lowering with the gate voltage.

Fig. 5 shows the current density versus the source-drain voltage  $V_D$  for structures with channel lengths  $L_{CH} = 20, 40$  nm. The solid lines represent the ballistic regime, the dashed and dotted lines reveal the effect of scattering due to ionized impurities, acoustic phonons and surface roughness at the Si/SiO<sub>2</sub> interface with an average displacement  $\Delta = 0.2$  nm and  $\Delta = 0.4$  nm respectively. At  $V_D = 0.2$  V we observe a kink in the  $I - V$  characteristic. For  $V_D < 0.2$  V the derivative  $V_D/I$  reflects the differential resistance of the structure. Obviously, the inclusion of the electron scattering mechanisms enhances the resistance of the structure and softens the kink in the  $I - V$  characteristic, thereby appreciably degrading the current in the MOSFET. The collisions play an especially important role for low source-drain voltages. The surface roughness at the Si/SiO<sub>2</sub> interface gives rise to an appreciable though not dominant contribution to the scattering in the channel. When  $V_D$  exceeds 0.2 V, a “saturation regime” is attained although the currents do not converge towards constant values. From Fig. 5 one may conclude that a decrease of the channel length leads to an increase of the  $I - V$  slope in the “saturation regime”. This result is a consequence of a reduction of the  $p-n$  junction barrier potential as the length of the channel becomes shorter.

Fig. 6 shows the  $I - V$  characteristics of the SOI MOSFET as a function of the gate voltage  $V_G$ . Fig. 7 illustrates the drain current  $I_D$  versus the gate voltage  $V_G$  of 30 nm channel-length SOI MOSFET for drain voltage  $V_D = 1$  V. We can see that the “threshold voltage” of the transistor is  $\simeq 0.0$  V. The influence of the scattering on the current diminishes as the gate voltage lowers. This fact is due to a reduced electron concentration resulting into a lower amplitude of the scattering process. The decrease of the electron concentration, together with an increasing source-channel junction barrier, leads to the reduction of the current through the channel. Fig. 7 also informs us that we are still far removed from the International Technology Roadmap for Semiconductors (ITRS) requirements<sup>40</sup>. In particular, whereas the on-state current ( $\simeq 5$  A/cm) is in the range of the requirements ( $\simeq 7.5$  A/cm), the off-state current (0.5 A/cm) is far above target ( $\simeq 0.0015$  A/cm). Therefore, further optimization of the silicon-film thickness as well as channel-doping engineering is needed.

In Fig. 8 the contours of the absolute value of the ground-state Wigner function ( $f_{11}$ ) are plotted with and without the presence of scattering for structures with channel lengths  $L_{CH} = 20$  nm (the first row), 30 nm (the second row), 40 nm (the third row). In these figures the first column corresponds to the ballistic regime, the second and the third correspond to the regime with scattering due to ionized impurities, acoustic phonons and surface roughness at the Si/SiO<sub>2</sub> interface with the average displacement  $\Delta = 0.2$  nm and  $\Delta = 0.4$  nm respectively. Darker areas in these plots indicate higher density of electrons. Far away from the  $p-n$  junctions where the effective potential is varying almost linearly with  $z$ , the partial Wigner function is positive definite and can be interpreted as a probability distribution of electrons in phase space. When electrons are accelerated in the inversion layer without scattering, their velocity increases monotonously along the whole channel. Therefore, in the phase-space representation, the distribution of ballistic electrons looks as a narrow jet stream pointing from the source to the drain along the channel, while scattering is seen to wash out the electron jet in the channel. Consequently, the electron transport through the channel combines the elements of both diffusive and ballistic motion. The mean-free-path less than the device length does not mean that the device is near-ballistic.

In this paper we have studied in detail the effects of ultra-short channels in an SOI MOSFET. To benefit from the SOI architecture, the thickness of the channel should be reduced to 10 nm or less. The simultaneous scaling of the channel length and thickness is currently under study.

### Acknowledgments

We acknowledge discussions with E. P. Pokatilov and S. N. Balaban. This work has been supported by the GOA BOF UA 2000, IUAP, FWO-V projects Nos. G.0306.00, G.0274.01N and the WOG WO.025.99N (Belgium).

### APPENDIX: SCATTERING MECHANISMS

We consider the electron scattering due to impurities, acoustic phonons and surface roughness at the Si-SiO<sub>2</sub> interface. In case of the electron scattering due to impurities<sup>34,41</sup>  $H_{\text{int}}$  is the electron-impurity potential minus its spatial average. The latter term has already been included in energy level calculations (band bending calculations), when solving Poisson and Wigner equations self-consistently. This spatial average being, by definition, translation invariant in the layer plane, has a zero matrix element between initial and final plane wave states and can thus be dropped. The impurities are assumed to be randomly placed at the sites  $\mathbf{R}_i \equiv (\boldsymbol{\rho}_i, z_i)$ . The Hamiltonian describing

scattering due to the impurities in the inversion layer is given by

$$\hat{H}_{\text{int}}(\mathbf{r}) = \sum_{\mathbf{q}} V_{\mathbf{q}}(z_i) \exp(i\mathbf{q}(\boldsymbol{\rho} - \boldsymbol{\rho}_i)), \quad (\text{A.1})$$

where

$$V_{\mathbf{q}}(z_i) = \frac{2\pi e^2}{\varepsilon_1(q + q_s F(q))} F(q, z_i). \quad (\text{A.2})$$

Here  $q_s$  is the Thomas-Fermi screening constant and  $F(q)$  and  $F(q, z_i)$  are form-factors, corresponding to the screening impurity potential<sup>29</sup>. Because the screening effect in the channel is very large, as seen in the Refs.<sup>30,31</sup>, we can model the scattering potential of an ionized impurity as  $U(\mathbf{r}) = (4\pi e^2 R_s^2 / \varepsilon_1) \delta(\mathbf{r})$ , where  $R_s$  determines a cross-section for scattering by an impurity. Consequently, the absolute value of the matrix element is

$$|\langle jsp'k' | U(\mathbf{r} - \mathbf{R}_i) | jspk \rangle| = 4\pi e^2 R_s^2 / \varepsilon_1 \psi_{js}^2(x_i, z_i). \quad (\text{A.3})$$

Averaging this over a uniform distribution of impurities results in the following scattering rate

$$P_{jspk, jsp'k'}^{\text{IM}}(z) = 2\pi C_{\text{IM}} \int_0^{L_x} dx \psi_{js}^4(x, z) \delta(E_{jsp'k'} - E_{jspk}), \quad (\text{A.4})$$

where

$$C_{\text{IM}} = \frac{1}{\hbar S} N_A \left( \frac{4\pi e^2 R_s^2}{\varepsilon_1} \right)^2, \quad (\text{A.5})$$

$N_A$  is the acceptor concentration and  $S = L_y L_z$ .

Lattice vibrations are an inevitable source of scattering, and we need to take them into account when we calculate device characteristics at room temperature. In this work we restrict ourselves to intra-valley and intra-subband acoustic phonon scattering. In the approximation of an isotropic elastic continuum we have

$$\hat{H}_{\text{int}}^{\text{e-ph}} = \Xi_u \left[ D \boldsymbol{\nabla} \cdot \mathbf{u}(\boldsymbol{\rho}, z) + \frac{\partial}{\partial z} u_z(\boldsymbol{\rho}, z) \right] = \sum_{\mathbf{q}} (\gamma_{\mathbf{q}} b_{\mathbf{q}} \exp(i\mathbf{q} \cdot \mathbf{r}) + h.c.), \quad (\text{A.6})$$

with<sup>42</sup>

$$|\gamma_{\mathbf{q}}|^2 = \frac{\hbar \Xi_u^2 q^2}{\rho V \omega_{\mathbf{q}}}.$$

$\Xi$ ,  $\rho$  and  $\omega_{\mathbf{q}}$  respectively denote the deformation potential, the mass density of the semiconductor and phonon frequency. The matrix elements describing single phonon emission and absorption processes are respectively given by

$$\langle jsp'k'; N_{\mathbf{q}} + 1 | \hat{H}_{\text{e-ph}} | jspk; N_{\mathbf{q}} \rangle = \gamma_{\mathbf{q}}^* \sqrt{N_{\mathbf{q}} + 1} \langle jsp'k' | \exp(-i\mathbf{q} \cdot \mathbf{r}) | jspk \rangle, \quad (\text{A.7})$$

$$\langle jsp'k'; N_{\mathbf{q}} - 1 | \hat{H}_{\text{e-ph}} | jspk; N_{\mathbf{q}} \rangle = \gamma_{\mathbf{q}} \sqrt{N_{\mathbf{q}}} \langle jsp'k' | \exp(i\mathbf{q} \cdot \mathbf{r}) | jspk \rangle, \quad (\text{A.8})$$

where  $N_{\mathbf{q}}$  is a phonon occupation number. The emission (+) and absorption (-) rates are

$$P_{jspk, jsp'k'}^+ = \frac{2\pi}{\hbar} \sum_{\mathbf{q}} |\gamma_{\mathbf{q}}|^2 (N_{\mathbf{q}} + 1) |\langle jsp'k' | \exp(-i\mathbf{q} \cdot \mathbf{r}) | jspk \rangle|^2 \delta(E_{jsp'k'} - E_{jspk} + \hbar\omega_{\mathbf{q}}), \quad (\text{A.9})$$

$$P_{jspk, jsp'k'}^- = \frac{2\pi}{\hbar} \sum_{\mathbf{q}} |\gamma_{\mathbf{q}}|^2 N_{\mathbf{q}} |\langle jsp'k' | \exp(i\mathbf{q} \cdot \mathbf{r}) | jspk \rangle|^2 \delta(E_{jsp'k'} - E_{jspk} - \hbar\omega_{\mathbf{q}}). \quad (\text{A.10})$$

At room temperature both expressions are approximately the same. Indeed, for  $T = 300$  K the thermal energy  $k_B T$  largely exceeds the phonon energy  $\hbar\omega_{\mathbf{q}}$ , and therefore the acoustic deformation can be considered elastic. For low

energies, we can approximate the phonon occupation number as  $N_{\mathbf{q}} \approx k_{\text{B}}T/\hbar\omega_{\mathbf{q}} \gg 1$  and adopt the Debye model  $\omega_{\mathbf{q}} = v_0 q$  where  $v_0$  is the sound velocity. Assuming equipartition of energy in the acoustic modes, we obtain the scattering rate :

$$P_{jspk,jsp'k'}^{\text{PH}}(z) = 2\pi C_{\text{PH}} \int_0^{L_x} dx \psi_{js}^4(x, z) \delta(E_{jsp'k'} - E_{jspk}), \quad (\text{A.11})$$

with

$$C_{\text{PH}} = \frac{1}{\hbar S} \Xi_{\text{u}}^2 \frac{k_{\text{B}}T}{\rho v_0^2}. \quad (\text{A.12})$$

Ideally, the Si-SiO<sub>2</sub> interfaces would coincide with a planes  $x = 0$  and  $x = t_{\text{Si}}$ . The real interfaces however are known to fluctuate randomly around these planes and, under the assumption that the boundary between Si and Si-SiO<sub>2</sub> is still abrupt, the local deviations due to surface roughness may be characterized by a quasi-continuous function  $\Delta(\boldsymbol{\rho})$ . Here  $\boldsymbol{\rho} = (y, z)$  represents the two-dimensional position vector parallel with the ideal interfaces. We further assume that the surface potential varies linearly with  $\Delta$ , i.e.

$$V(x + \Delta(\boldsymbol{\rho})) \approx V(x) + \Delta(\boldsymbol{\rho}) \frac{\partial V(x)}{\partial x}. \quad (\text{A.13})$$

Neglecting the effect of surface roughness on the subband energies and wave functions, we may calculate the scattering matrix element for surface roughness to the lowest order in  $\Delta$  as follows<sup>29,43</sup>:

$$\langle jspk | \hat{H}_{\text{int}}^{\text{SR}} | jsp'k' \rangle = \frac{\hbar^2}{2m_j^{\text{xx}}} \left. \frac{\partial \psi_{js}}{\partial x} \frac{\partial \psi_{js}}{\partial x} \right|_{x=0} \Delta_{\mathbf{k}-\mathbf{k}'} = \Delta_{\mathbf{k}-\mathbf{k}'} \int_0^{L_x} dx |\psi_{js}|^2 \frac{\partial V(x)}{\partial x}, \quad (\text{A.14})$$

where  $\mathbf{k} \equiv (k, p)$  and  $\Delta_{\mathbf{k}-\mathbf{k}'}$  is the Fourier transform of the  $\Delta(\boldsymbol{\rho})$

$$\Delta(\boldsymbol{\rho}) = \sum_{\mathbf{q}} \Delta_{\mathbf{q}} \exp(i\mathbf{q} \cdot \boldsymbol{\rho}). \quad (\text{A.15})$$

In the Born approximation, only the magnitude squared of  $\Delta_{\mathbf{k}-\mathbf{k}'}$  (referred to as the power spectrum) is needed, and thus the phase of  $\Delta_{\mathbf{k}-\mathbf{k}'}$  can be neglected. We propose a Gaussian distribution to describe the spatial correlation of the surface roughness

$$C(\boldsymbol{\rho} - \boldsymbol{\rho}') = \langle \Delta(\boldsymbol{\rho}) \Delta(\boldsymbol{\rho}') \rangle = \Delta^2 \exp\left(-\frac{|\boldsymbol{\rho} - \boldsymbol{\rho}'|^2}{\Lambda^2}\right), \quad (\text{A.16})$$

where  $\Delta$  is the root-mean-square value of  $\Delta(\boldsymbol{\rho})$ , and  $\Lambda$ , is referred to as the correlation length governing the the decay of the auto-correlation function. In the above expression the brackets  $\langle \rangle$  denote sample averages<sup>29</sup>. By convolution, the power spectrum reduces to the Fourier transform of the auto-correlation function (A.16), that is given by

$$S(\mathbf{q}) = |\Delta_{\mathbf{q}}|^2 = \pi \Delta^2 \Lambda^2 \exp(-\mathbf{q}^2 \Lambda^2 / 4) \quad (\text{A.17})$$

and where  $\mathbf{q}$  is the scattered wave vector.

Consequently, the interface roughness scattering rate takes the form :

$$P_{jspk,jsp'k'}^{\text{SR}}(z) = \frac{2\pi^2}{\hbar S} \Delta^2 \Lambda^2 \exp\left(-\frac{|\mathbf{k} - \mathbf{k}'|^2 \Lambda^2}{4}\right) \left[ \int_0^{L_x} dx |\psi_{js}(x, z)|^2 \frac{\partial V(x)}{\partial x} \right]^2 \times \delta(E_{jsp'k'} - E_{jspk}). \quad (\text{A.18})$$

The total scattering rate

$$P_{jspk,jsp'k'} = P_{jspk,jsp'k'}^{\text{IM}} + P_{jspk,jsp'k'}^{\text{PH}} + P_{jspk,jsp'k'}^{\text{SR}} \quad (\text{A.19})$$

is then inserted into Eq. (26) in order to obtain the one-dimensional scattering rate

$$P_{js}^{\text{IM+PH}}(z, k, k') = \left( m_j^{\text{yy}} \frac{2L_y^2 \beta}{\hbar^2 \pi} \right)^{\frac{1}{2}} (C_{\text{IM}} + C_{\text{PH}}) F\left(\beta \frac{\hbar^2 k^2}{2m_j^{\text{zz}}} - \beta \frac{\hbar^2 k'^2}{2m_j^{\text{zz}}}\right) \int_0^{L_x} \psi_{js}^4(x, z) dx, \quad (\text{A.20})$$

$$P_{js}^{\text{SR}}(z, k, k') = \frac{\pi}{\hbar S} \Delta^2 \Lambda^2 \left( m_j^{\text{yy}} \frac{2L_y^2 \beta}{\hbar^2 \pi} \right)^{\frac{1}{2}} \exp \left( -\frac{(k - k')^2 \Lambda^2}{4} \right) \times \\ \Pi(k^2 - k'^2) \left[ \int_0^{L_x} dx |\psi_{js}(x, z)|^2 \frac{\partial V(x)}{\partial x} \right]^2, \quad (\text{A.21})$$

where

$$\Pi(x) = \int_0^\infty dp \frac{\exp \left[ -\beta \frac{\hbar^2 p^2}{2 \sqrt{m_j^{\text{zz}} m_j^{\text{yy}}}} \right]}{\sqrt{p^2 + x}} \times \\ \left[ \exp \left( -\frac{\left( p - \sqrt{p^2 + x} \right)^2 \Lambda^2}{4 \sqrt{\frac{m_j^{\text{zz}}}{m_j^{\text{yy}}}}} \right) + \exp \left( -\frac{\left( p + \sqrt{p^2 + x} \right)^2 \Lambda^2}{4 \sqrt{\frac{m_j^{\text{zz}}}{m_j^{\text{yy}}}}} \right) \right], \quad (\text{A.22})$$

$$F(x) = {}^{-x/2} K_0(|x|/2), \quad (\text{A.23})$$

and  $K_0(x)$  is a McDonald function<sup>44</sup>.

- 
- <sup>†</sup> Permanent address: Department of Theoretical Physics, State University of Moldova, str. A. Mateevici 60, MD-2009 Kishinev, Republic of Moldova.
- <sup>‡</sup> Also at: Universiteit Antwerpen (RUCA), Groenenborgerlaan 171, B-2020 Antwerpen, Belgium and Technische Universiteit Eindhoven, P. B. 513, 5600 MB Eindhoven, The Netherlands.
- <sup>1</sup> S. M. Sze, *Physics of Semiconductor Devices* (John Wiley and Sons, New York, 1981).
  - <sup>2</sup> D. J. Frank, Y. Taur and H.-S. P. Wong, IEEE Electron Dev. Lett. **10**, 385 (1998).
  - <sup>3</sup> L. V. Keldysh, Zh. Eksp. Teor. Fiz. **47**, 1515 (1964) [Sov. Phys. JETP **20**, 1018 (1965)].
  - <sup>4</sup> L. P. Kadanoff and G. Baym, *Quantum Statistical Mechanics* (Benjamin, New York, 1962).
  - <sup>5</sup> W. Hänsch and G. D. Mahan, Phys. Rev. B **28**, 1902 (1983).
  - <sup>6</sup> A. P. Jauho and J. W. Wilkins, Phys. Rev. B **29**, 1919 (1984).
  - <sup>7</sup> S. Sarker, Phys. Rev. B **32**, 743 (1985).
  - <sup>8</sup> A. P. Jauho, Phys. Rev. B **32**, 2248 (1985).
  - <sup>9</sup> S. Datta, Superlattices and Microstructures **28**, 253 (2000).
  - <sup>10</sup> S. Datta, *Electronic transport in Mesoscopic Systems* (Cambridge University Press, Cambridge, UK, 1997).
  - <sup>11</sup> Z. Ren, R. Venigopal, S. Datta, and M. Lunstrom, IEDM Tech. Digest, Washington, D.C., Dec. 3-5, 2001.
  - <sup>12</sup> M. Lundstrom, Z. Ren, IEEE Trans. Electron Devices **49**, 133 (2002).
  - <sup>13</sup> M. V. Fischetti, J. Appl. Phys. **83**, 270 (1998).
  - <sup>14</sup> M. V. Fischetti, Phys. Rev. B **59**, 4901 (1999).
  - <sup>15</sup> F. Castella, J. Stat. Phys. **104**, 387 (2001).
  - <sup>16</sup> R. Brunetti, C. Jacoboni, and F. Rossi, Phys. Rev. B **39**, 10781 (1989).
  - <sup>17</sup> C. Jacoboni, Semicond. Sci. Technol. **7**, B6 (1992); in *Quantum Transport in Semiconductors*, edited by D. K. Ferry and C. Jacoboni (Plenum, New York, 1992), p.1.
  - <sup>18</sup> U. Ravaioli, M. A. Osman, W. Pötz, N. C. Kluksdhal and D. K. Ferry, Physica B **134**, 36 (1985).
  - <sup>19</sup> W. Frensley, Phys. Rev. B **36**, 1570 (1987).
  - <sup>20</sup> N. C. Kluksdahl, A. M. Krivanek, D. K. Ferry, and C. Ringhofer, Phys. Rev. B **39**, 7720 (1989).
  - <sup>21</sup> F. A. Buot and K. L. Jensen, Phys. Rev. B **42**, 9429 (1990).
  - <sup>22</sup> W. Frensley, Rev. Mod. Phys. **62**, 745 (1990).
  - <sup>23</sup> H. Tsuchiya, M. Ogawa, and T. Miyoshi, Jpn. J. Appl. Phys. **30**, 3853 (1991).
  - <sup>24</sup> S. N. Balaban, E. P. Pokatilov, V. M. Fomin, V. N. Gladilin, J. T. Devreese, W. Magnus, W. Schoenmaker, M. Van Rossum and B. Sorée, Solid-St. Electron. **46**, 435 (2002).
  - <sup>25</sup> T. Mizuno, R. Ohba, and K. Ohuchi, Appl. Phys. Lett. **69**, 106 (1996).
  - <sup>26</sup> Y. Nakajima, Y. Takahashi, S. Horiguchi, K. Iwade, H. Namatsu, K. Kurihara and M. Tabe, Appl. Phys. Lett. **65**, 2833 (1994).
  - <sup>27</sup> H.-W. Lee, Physics Reports **259**, 147 (1995).
  - <sup>28</sup> P. Bordone, M. Pascoli, R. Brunetti, A. Bertoni, and C. Jacoboni, Phys. Rev. B **59**, 3060 (1998).
  - <sup>29</sup> T. Ando, A. B. Fowler, and F. Stern, Rev. Mod. Phys. **54**, 437 (1982).
  - <sup>30</sup> M. Lundstrom, *Fundamentals of carrier transport* (Cambridge University Press, Cambridge, UK, 2000).
  - <sup>31</sup> E. P. Pokatilov, V. M. Fomin, S. N. Balaban, V. N. Gladilin, S. N. Klimin, J. T. Devreese, W. Magnus, W. Schoenmaker, N. Collaert, M. Van Rossum and K. De Meyer, J. Appl. Phys. **85**, 6625 (1999).
  - <sup>32</sup> Carriers within the active device region are injected either from the source reservoir or the drain reservoir. Both reservoirs are assumed in the equilibrium state, characterized by different Fermi energy levels.
  - <sup>33</sup> A. Isihara, *Statistical Physics* (State University of New York, Buffalo, Academic Press, New York – London, 1971).
  - <sup>34</sup> P. Carruthers, F. Zachariasen, Rev. Mod. Phys. **55**, 245 (1983).
  - <sup>35</sup> L. I. Schiff, *Quantum mechanics* (McGraw-Hill, New York, 1968).
  - <sup>36</sup> K. L. Jensen and A. K. Ganguly, J. Appl. Phys. **73** (1993).
  - <sup>37</sup> S. M. Goodnick, D. K. Ferry, C. W. Wilmsen, Z. Liliental, D. Fathy and O. L. Krivanek, Phys. Rev. B **32**, 8171 (1985).
  - <sup>38</sup> M. L. Green, E. P. Gusev, R. Degraeve, and E. L. Garfunkel, J. Appl. Phys. **90**, 2057 (2001).
  - <sup>39</sup> K. H. Hellwege, Landolt-Börnstein, editors. Semiconductors. Physics of II-VI and I-VII Compounds, Semimagnetic Semiconductors, vol. 17, New Series, Group III (Springer, Berlin, 1982).
  - <sup>40</sup> The International Technology Roadmap for Semiconductors: 2001 document edited by International SEMATECH, URL <http://www.sematech.org>
  - <sup>41</sup> D. Chattopadhyay and H. J. Queisser, Rev. Mod. Phys. **53**, 745 (1981).
  - <sup>42</sup> P. D. Yoder, V. D. Natoli and R. M. Martin, J. Appl. Phys. **73**, 4378 (1993).
  - <sup>43</sup> R. E. Prange, T.-W. Nee, Phys. Rev. **168**, 779 (1968).
  - <sup>44</sup> M. Abramowitz and I. Stegun (Eds.), *Handbook of Mathematical Functions with Formulas, Graphs, and Mathematical Tables* (National Bureau of Standards, Washington, DC, 1972).

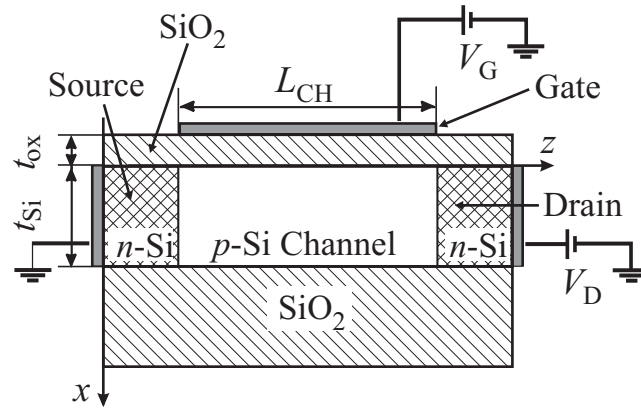


FIG. 1: Scheme of the SOI MOSFET.

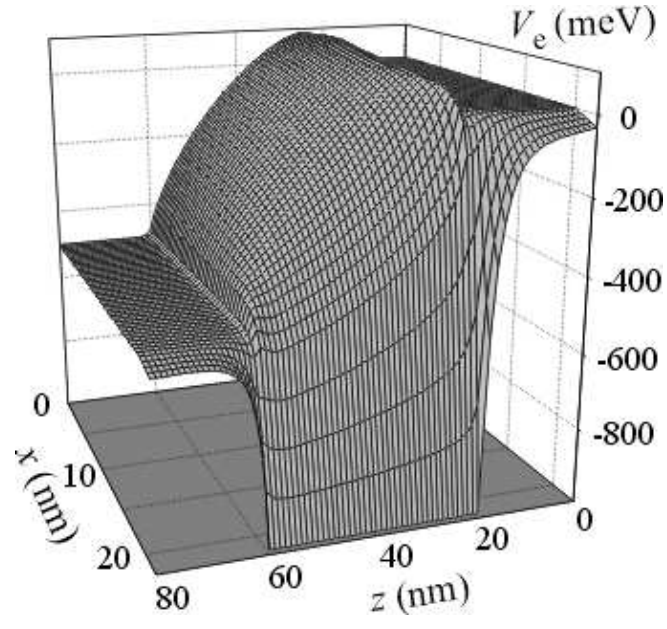


FIG. 2: The electrostatic potential energy in the SOI MOSFET with  $L_{CH} = 40$  nm at  $V_G = 1$  V and  $V_D = 0.5$  V.

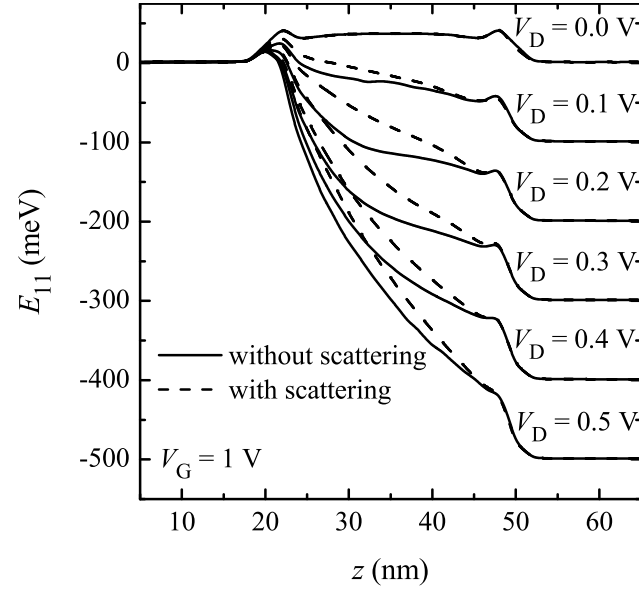


FIG. 3: Effective potential as a function of  $z$  for various  $V_D$ ,  $L_{CH} = 30$  nm.



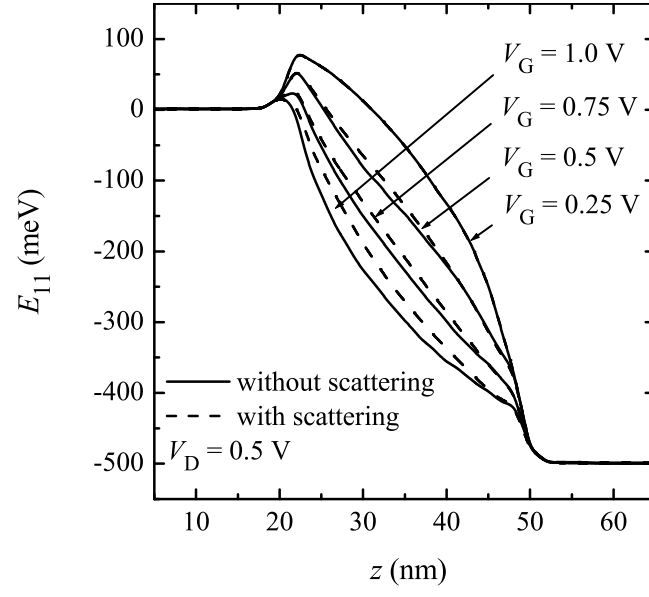


FIG. 4: Effective potential as a function of  $z$  for various  $V_G$ ,  $L_{CH} = 30$  nm.

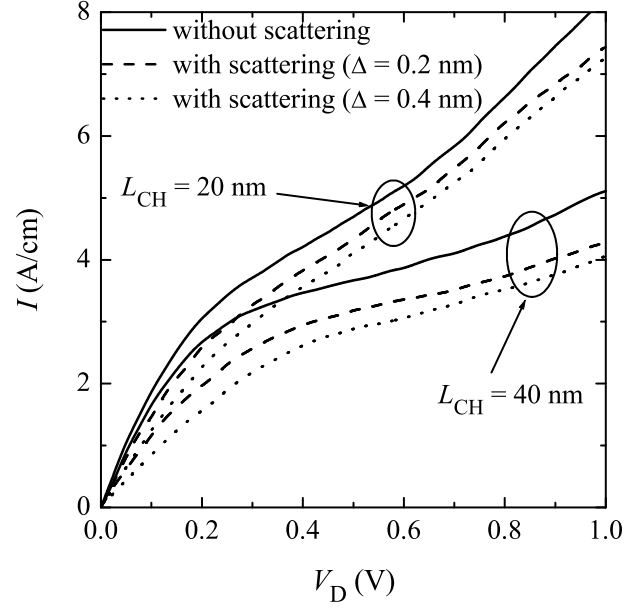


FIG. 5: Current-voltage characteristics at  $V_G = 1$  V for different channel lengths.

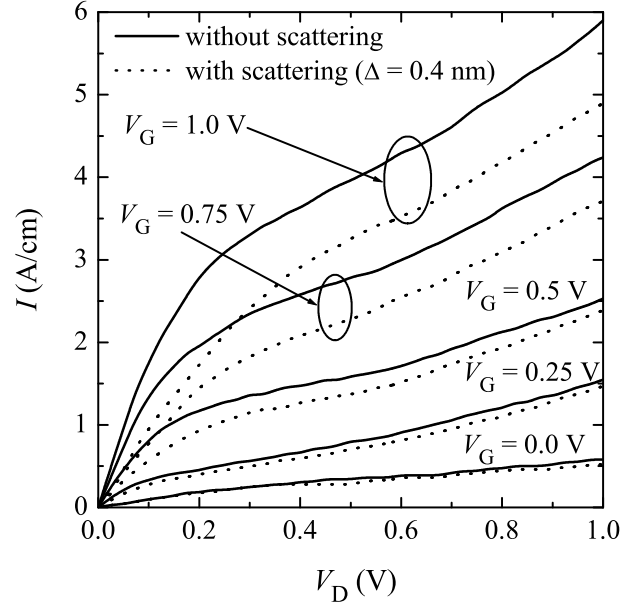


FIG. 6: Current-voltage characteristics for SOI MOSFET with  $L_{CH} = 30$  nm.

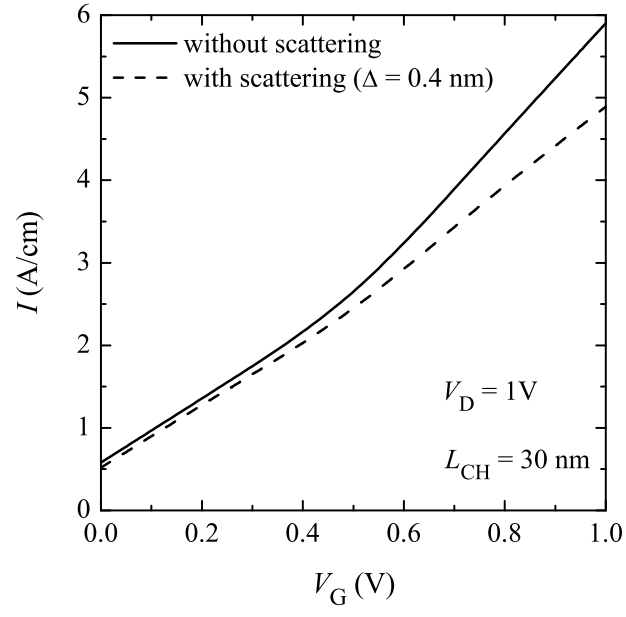


FIG. 7: Drain current vs. gate voltage characteristics for drain voltage  $V_D = 1$  V.

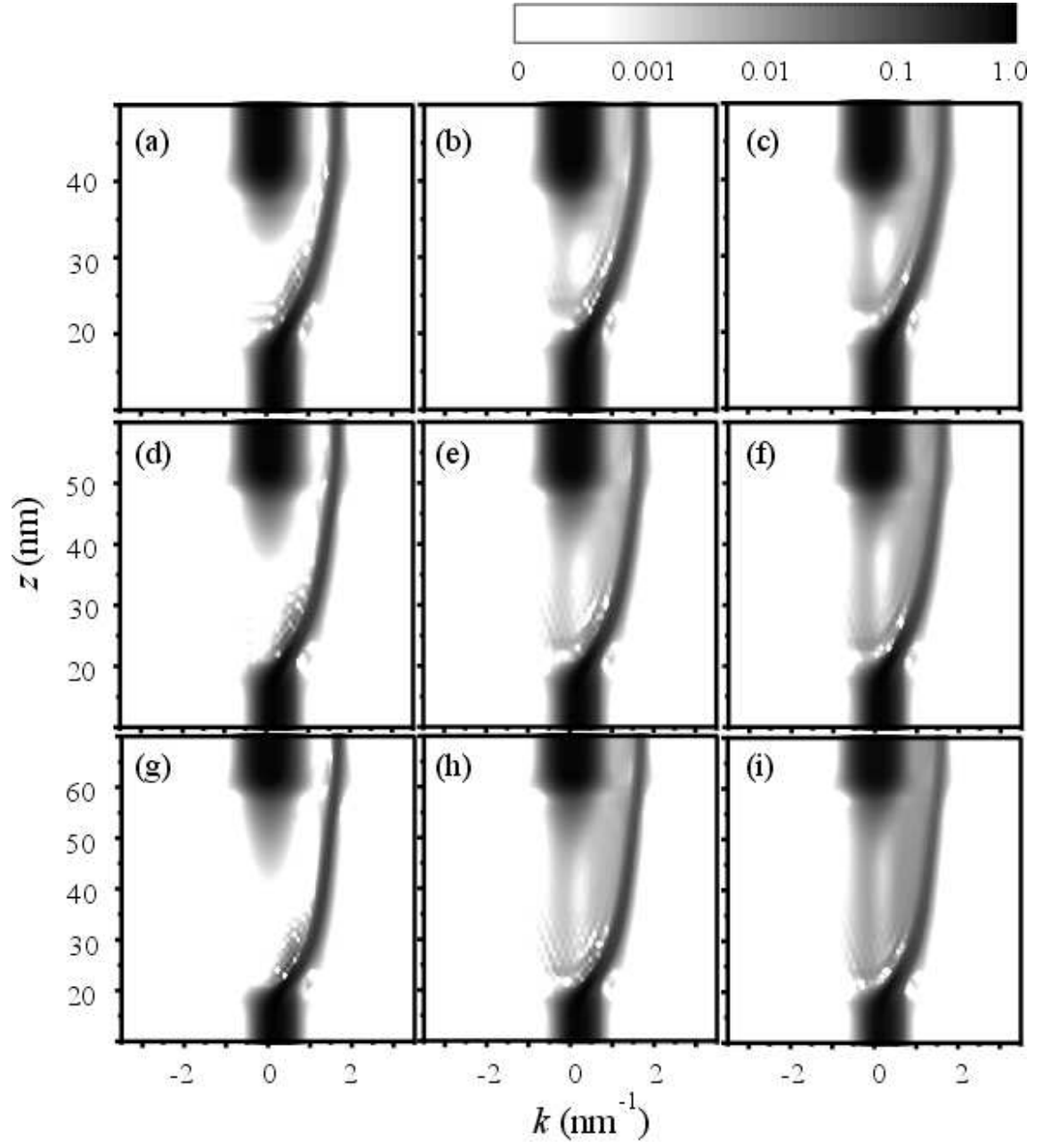


FIG. 8: Contour plots of the absolute value of the partial Wigner distribution function  $|f_{11}(z, k)|$  at  $V_G = 1$  V,  $V_D = 0.5$  V and various channel length.  $L_{CH} = 20$  nm: (a) without scattering, (b) with scattering  $\Delta = 0.2$  nm, (c) with scattering  $\Delta = 0.4$  nm;  $L_{CH} = 30$  nm: (d) without scattering, (e) with scattering  $\Delta = 0.2$  nm, (f) with scattering  $\Delta = 0.4$  nm;  $L_{CH} = 40$  nm: (g) without scattering, (h) with scattering  $\Delta = 0.2$  nm, (i) with scattering  $\Delta = 0.4$  nm.